2011 IEEE/RSJ International Conference on
Intelligent Robots and Systems
September 25-30, 2011. San Francisco, CA, USA

Avoiding steering actuator saturation in off-road mobile robot path tracking via predictive velocity control

Oliver Hach[1], Roland Lenain[1], Benoit Thuilot[2,4], Philippe Martinet[3,4]
[1] Cemagref, 24 avenue des Landais, 63172 Aubière, France
[2] Clermont Université, Université Blaise Pascal, LASMEA, BP 10448, 63000 Clermont-Ferrand, France
[3] Clermont Université, IFMA, LASMEA, BP 10448, 63000 Clermont-Ferrand, France
[4] CNRS, UMR 6602, LASMEA, 63177 Aubière, France
{oliver.hach, roland.lenain}@cemagref.fr benoit.thuilot@lasmea.univ-bpclermont.fr

***Abstract*— In mobile robot path tracking applications, an autonomous vehicle is steered to stay as close as possible to a desired path. If lateral wheel slip is an important variable, as it is the case at high speed and due to low tire-ground friction in off-road applications, limits of the steering actuators, the major input constraints of the system, have a major influence on the tracking control performance. This paper presents an algorithm to control the longitudinal velocity, a secondary control variable, of a mobile robot in order to respect the boundedness of the steering angle, and thus to improve the vehicle safety. The applicability of the algorithm has been verified through experiments with an off-road mobile robot.**

I. Introduction

Path tracking for wheeled mobile robots under off-road conditions is a complex problem, especially at high speed. Low and variable grip consitions causes non-negligible wheel slip, possibly leading to a loss of the vehicle controllability or integrity, when it spins or leaves the desired path. To overcome the problems of entirely kinematic [1, e.g.] or dynamic approaches [2, e.g.], a mixed kinematic-dynamic control technique has been proposed for off-road path tracking at high speed (see [3], [4]). It uses a kinematic control law in combination with dynamic observation strategies and achieves highly accurate path following. However, depending on tire-ground friction, the reference path's shape and the targeted vehicle speed, the existing control strategy can not always maintain the vehicle's integrity nor guarantee accurate tracking. A major cause of this shortcoming is the mechanical steering angle limit of the high speed off-road mobile robot platform (Fig. 1), i.e. the boundedness of the system input. While a trajectory can be be attainable at low speed, it might become unachievable at higher speed, because lateral slip of the vehicle leads to different turning radii at the same steering angle δ, depending on the platform speed and the actual friction conditions.

The problem of input constraints of mobile robots has been addressed on the motion planning level and in terms of control by various approaches. In [5] kinematic vehicle and input constraints are treated via predictive potential fields. A path planning strategy that respects kinematic and dynamic constraints of a mobile robot was shown in [6]. Wheeled mobile robots were used in [7] to study trajectory following of Unmanned Aerial Vehicles, that are subject to important motion constraints, where constraint Lyapunov functions are employed to create saturation controllers to respect velocity constraints. In [8] chained form controllers for wheeled mobile robots have been proposed that account for input saturation. However, these approaches either do not respect dynamic constraints or they suffer from the possibility to adapt to varying operating conditions, that are inevitable prerequisites in off-road applications.

The algorithm presented in this paper aims on the complement of the existing control system, shortly summarized in section II, by a limitation of the steering angle, accomplished via a modulation of the linear velocity. For this purpose, the speed dependent cornering behavior of the robot is used to generate a desired profile of the robot's velocity, taking into account the current tire-ground friction conditions. Predictive Functional Control (PFC) is employed to control the vehicle speed with respect to this profile (section III). Section IV shows experimental results obtained on the robot platform depicted in Fig. 1.

Fig. 1. Experimental off-road robot platform

II. Existing hybrid path tracking control

This section recapitulates the existing hybrid path tracking control law, that is complemented by the velocity limitation algorithm. It is specifically designed for off-road applications of car-like mobile robots.

A. Extended kinematic model

Because dynamic model based control laws have certain drawbacks in off-road path tracking - first of all the high variability of the system parameters that often

TABLE I

PRINCIPAL SYMBOLS

β, β_F, β_R	vehicle side-slip angles (global, front, rear)
θ	vehicle yaw angle
m, I_z	Robot mass and vertical inertia
$C_{F,R}$	cornering stiffnesses
v, v_t, v_d	robot velocity, target velocity, desired limit
$L_F + L_R = L$	wheelbase and longitudinal position of CoG
δ	front steering angle
Γ	reference path
a	curvilinear abscissa, length of the path
$c(a)$	curvature of the path at a

leads to oscillating behavior - the current control scheme is based on a kinematic formulation of the control system. The kinematic vehicle model [1, e.g.] is therefore extended by integrating the side-slip of the vehicle. With the controlled variables y (the distance of the robot from the path) and $\tilde{\theta}$ (the difference between the robot's orientation and the path's tangent, see Fig. 2), the side-slip angles $\beta_{R,F}$, the linear velocity v, the curvature of the reference path $c(a)$ and the front steering angle δ, the system can be modeled with respect to the curvilinear abscissa a (as detailed in [9]) as:

$$\begin{cases} \dot{a} &= v\frac{\cos(\tilde{\theta}+\beta_R)}{1-c(a)\,y} \\ \dot{y} &= v\sin(\tilde{\theta}+\beta_R) \\ \dot{\tilde{\theta}} &= v\left[\cos(\beta_R)\lambda_1 - \lambda_2\right] \end{cases} \tag{1}$$

where

$$\lambda_1 = \frac{\tan(\delta+\beta_F) - \tan(\beta_R)}{L},\ \lambda_2 = \frac{c(a)\cos\tilde{\theta} + \beta_R}{1-c(a)y}$$

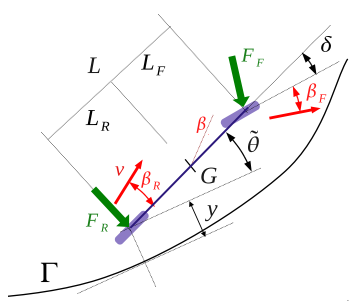

Fig. 2. Path tracking parameters

B. Observation of grip conditions

As model (1) reveals, the knowledge of the side-slip angles β_F and β_R is of crucial importance. These angles are hardly measurable directly, thus a mixed mode observation scheme has been proposed in [9] and recently improved in [4]. It consists of a three step process, involving kinematic and dynamic models.

1) A kinematic observation, based on model (1), estimates the side-slip angles β_F and β_R precisely, yet rather slow, because dynamic variables are deduced from kinematic models and measurements.
2) This estimate of the side-slip allows the adaptation of the cornering stiffnesses C_F and C_R, representing the current grip conditions via the linear tire model (2), that relates the lateral tire forces $F_{F,R}$ to $\beta_{F,R}$. Since C_F and C_R are adapted on-line, changing grip conditions and nonlinear friction effects are reflected by the model. This method has been chosen because of the different physical effects involved. Precise off-road tire modelling leads inevitably to complex formulae with many parameters, making them unsuitable for on-line estimation algorithms.
3) Using these estimates of the cornering stiffness and an additional measurement of the vehicle yaw rate, a dynamic side-slip observer is set up. It allows for faster convergence than the kinematic observation.

$$\begin{cases} F_F &= C_F(.)\,\beta_F \\ F_R &= C_R(.)\,\beta_R \end{cases} \tag{2}$$

This mixed-model observation approach, combining a direct kinematic observation in step 1) and the reactivity of dynamic models in the steps 2) and 3), provides estimates of the important vehicle parameters: the side-slip angles $\beta_{F,R}$, and the cornering stiffnesses $C_{F,R}$. Thanks to this observer, the cornering stiffnesses are on-line adapted, accounting for both the contact nonlinearity and the variation of grip conditions.

C. Adaptive and predictive control law

Now the estimated parameters permit the construction of a control law, based on the extended kinematic model (1). Via exact linearization, (3) can be set up with the positive gains K_p and K_d. The geometric approach yields a kinematic, time (and thus speed) independent controller with exponential convergence of the vehicle to the desired path by tuning the law's gains to attain a desired settling distance.

$$\delta = \arctan\left(\tan(\beta_R) + \frac{L}{\cos(\beta_R)}\left(\frac{c(a)\cos\tilde{\theta}_1}{\alpha} + \frac{A\cos^3\tilde{\theta}_1}{\alpha^2}\right)\right) - \beta_F \tag{3}$$

with

$$\begin{cases} \tilde{\theta}_1 &= \tilde{\theta} + \beta_R \\ \alpha &= 1 - c(a)y \\ A &= -K_p\,y - K_d\,\alpha\tan\tilde{\theta}_1 + c(a)\alpha\tan^2\tilde{\theta}_1 \end{cases}$$

In order to compensate for delays in the low level control of the robot, control law (3) is split into two parts: a reactive part, mainly depending on the robot's deviation from the reference path, and a predictive part, mainly depending on its curvature $c(a)$ (that is known in advance). Their sum $\delta = \delta_{Traj} + \delta_{Dev}$ is then applied as target value in a model predictive controller (see [9] for details), whose horizon (the amount of prediction time used) is adjusted to the low level control's properties. Thus, steering commands are sent in advance and the vehicle's yaw corresponds to the curvature of the path.

D. Performance and limitations

The adaptive and predictive control law obtains precise path tracking under different and varying grip conditions. Maximum lateral errors between 0.1 m (at $3\,\mathrm{m\,s^{-1}}$) and 0.5 m (at $6\,\mathrm{m\,s^{-1}}$) can be achieved.

Nonetheless there are two major limitations:

1) Due to unmodeled process dynamics, the tracking controller gains and the horizon of the predictive steering control need to be adjusted with respect to the target longitudinal vehicle speed v_t to achieve optimal results.
2) The reference path Γ is generated by manually steering the robot at low speed. Kinematically it can thus be followed without doubt. However, dynamically the path can be unachievable, depending on the current friction conditions and the targeted vehicle speed v_t, because the physically limited angle of the steering actuator constraints the robot's motion.

III. Velocity limitation

The existing control law acts on the robot's primary control variable: the steering angle. As the limitation algorithm is designed to complement the steering control, it has to act on the secondary control variable, the vehicle speed. In this section an expression is derived that relates vehicle speed, steering angle and turning radius during cornering. Due to lateral wheel slip, the same steering angle results in different radii when the vehicle velocity is different.

A. Relation of steering angle, speed and turning radius in a steady-state curve

To obtain this expression, the linear lateral dynamic bicycle model (4) is employed, that is frequently used to represent the lateral vehicle behavior (assuming that the angles δ and β are small). Likewise, it is the base for the the dynamic observation outlined in section II-B:

$$\dot{x} = Ax + B\delta \tag{4}$$

with

$$A = \begin{pmatrix} -\frac{C_F+C_R}{m\,v} & -\frac{m\,v^2+C_FL_F-C_RL_R}{m\,v^2} \\ -\frac{C_FL_F-C_RL_R}{I_z} & -\frac{C_FL_F^2+C_RL_R^2}{I_zv} \end{pmatrix}$$

$$B = \begin{pmatrix} \frac{C_F}{m\,v} & \frac{C_FL_F}{I_z} \end{pmatrix}^T$$

and the state vector

$$x = \begin{pmatrix} \beta & \dot{\theta} \end{pmatrix}^T$$

In the static equilibrium ($\dot{x} = 0$) system (4) becomes:

$$-\frac{C_F+C_R}{m\,v}\beta - \frac{m\,v^2+C_FL_F-C_RL_R}{m\,v^2}\dot{\theta} + \frac{C_F}{m\,v}\delta = 0 \tag{5}$$

$$-\frac{C_FL_F-C_RL_R}{I_z}\beta - \frac{C_FL_F^2+C_RL_R^2}{I_zv}\dot{\theta} + \frac{C_FL_F}{I_z}\delta = 0 \tag{6}$$

Solving (5) for β and inserting the result in (6) yields:

$$\frac{\dot{\theta}}{\delta} = \frac{v\,C_FC_R\,(L_F+L_R)}{C_FC_R\,(L_F+L_R)^2 - m\,v^2(C_FL_F-C_RL_R)} \tag{7}$$

On the supposition that the path is well tracked, its curvature $c(a)$ can be assumed to be identical to the inverse of the turning radius: $c(a) = \frac{\dot{\theta}}{v}$. By solving (7) for v, the desired relation (8) between vehicle velocity and steering angle is achieved for constant grip conditions.

$$\boxed{v(a) = \left(\frac{C_FC_R\,L\,\left(L\,c(a)-\delta\right)}{c(a)\,m\,(C_FL_F-C_RL_R)}\right)^{1/2}} \tag{8}$$

The singularities of (8) will be addressed in section III-B. As an illustration, for the parameters of the experimental platform ($L_R = 0.65\,\mathrm{m}$, $L_F = 0.55\,\mathrm{m}$, $m = 400\,\mathrm{kg}$), considering an identical cornering stiffness for front and rear axle and a constant steering angle, the vehicle needs to be slower at lower grip to attain the same curvature. For instance, the robot would have to travel at $3.43\,\mathrm{m\,s^{-1}}$ to attain a curvature of $0.15\,\mathrm{m^{-1}}$ at $\delta = 12°$ if $C_{F,R} = 2000\,\mathrm{N\,rad^{-1}}$, it would have to travel at $7.67\,\mathrm{m\,s^{-1}}$ if $C_{F,R} = 10\,000\,\mathrm{N\,rad^{-1}}$.

Relation (8) exhibits interesting properties, related to the vehicle's steering behavior, that are further discussed in the sequel.

B. Velocity limitation via equilibrium speed

Equation (8) becomes singular in the following cases:

1) $c(a) = 0$
2) $d_s = C_FL_F - C_RL_R = 0$
3) the square root radical is negative

Case 1) of zero curvature is a conceptual singularity, there is no speed associated to a straight line motion and there is no need for its limitation. The singularities of the cases 2) and 3) are directly related to the vehicle's current steering behavior.

In the kinematic case the linear model defines a relation of curvature and steering angle:

$$c = {}^{\delta}/_{L} \tag{9}$$

The expression is a linearized version of the geometric relation $c = {}^{\tan(\delta)}/_{L}$ of the vehicle kinematics. In the linear kinematic case, a path is then "kinematically admissible" if:

$$c_{max} < {}^{\delta_{max}}/_{L} \tag{10}$$

In order to incorporate the side-slip of a vehicle, (7) is reorganized (again assuming $c = {}^{\dot{\theta}}/_{v}$) to define the dynamic equivalent to (9):

$$\begin{aligned} c &= \frac{C_FC_RL}{C_FC_RL^2 - mv^2(C_FL_F-C_RL_R)}\,\delta \\ &= \frac{\delta}{L - \frac{mv^2d_s}{C_FC_RL}} \end{aligned} \tag{11}$$

Now two different cases have to be distinguished:

- understeer, $d_s < 0$: the effective steady-state turning radius of the vehicle is lower than kinematically defined by ${}^{\delta}/_{L}$, as yielding from (11)

- oversteer, $d_s > 0$: the effective steady-state turning radius of the vehicle is higher than kinematically defined by δ/L, as (11) reveals

This difference is important for the applicability of the equilibrium speed to velocity limiting. Likewise important is the fact that the steering behavior is not an inherent property of a vehicle. It is significantly depending on the present grip conditions.

The singular cases 2) and 3) of (8) are interpreted under distinction of the steering behavior:

- understeer: The square root radical is positive if $c < \delta/L$, which is always the case for understeer. Equation (11) reveals that the robot's velocity has to be reduced in the presence of slip, in order to achieve curves close to the kinematic case. A curve thus is dynamically admissible, if it is kinematically admissible (although $v = 0$). For $v > 0$ the "dynamic admissibility" can be be defined in analogy to (10) as:

$$c_{max} < \frac{C_F C_R L}{C_F C_R L^2 - m v^2 (C_F L_F - C_R L_R)} \, \delta_{max} \tag{12}$$

- oversteer: The square root radical is positive if $c > \delta/L$, which is always ensured for oversteer. Any curvature can be achieved, since for smaller values of c the steering angle δ can be adapted.
- neutral: At the margin between understeer and oversteer ($d_s = 0$), (8) becomes singular, because the velocity has no influence on the cornering behavior. (12) becomes identical to (10), a curve is dynamically admissible, if it is kinematically admissible.

Our experimental robot platform normally understeers. In order to assure the dynamic admissibility of the reference path, a velocity limit profile v_d can be calculated according to (8) with respect to a desired steering angle limit δ_{max}. The evaluation is based on the observed front and rear cornering stiffnesses $C_{F,R}$ (wich are on-line adapted thanks to the observer introduced in section II-B) and future curvature values of the learned reference path.

According to experience, at high speed the probability of oversteer increases due to more important wheel slip and important steering angles. The robot then risks to spin, whereby the vehicle's integrity is lost. For vehicles exposing this behavior, a velocity limitation helps to avoid the transition to oversteer.

This property might seem to be a contradiction to the discussion above, where oversteer appears to have advantages to understeer, because the turning radius of the robot is not limited. The transition from understeer to oversteer occurs at low grip due to different friction conditions on the front and rear axle of the robot. Even if the side-slip angles become important in this situation and the linear bicycle model is not longer a precise system description, (8) provides an idea of the associated risk. Fig. 3 shows the the equilibrium speed for differing C_F and C_R ($\delta = 10°$, $C_F = 2000\,\mathrm{N\,rad^{-1}}$, $L_F = 0.55\,\mathrm{m}$, $L_R = 0.65\,\mathrm{m}$). It is clearly visible that small variations in speed can cause high variations in curvature, when the steering behavior passes from understeering ($C_R = 2000\,\mathrm{N\,rad^{-1}}$ and $C_R = 1800\,\mathrm{N\,rad^{-1}}$) to oversteering ($C_R = 1600\,\mathrm{N\,rad^{-1}}$ and $C_R = 1400\,\mathrm{N\,rad^{-1}}$). In this context, it is important to note that the cornering stiffnesses are not a static property of the tire-soil interaction. Due to nonlinear friction effects, these parameters are highly variable.

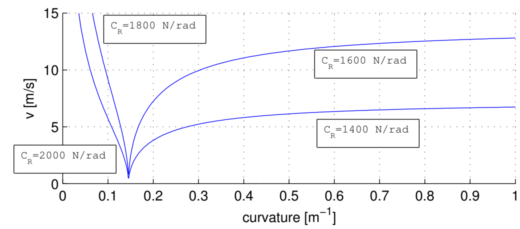

Fig. 3. Example of possible transition from understeer to oversteer

C. Model predictive longitudinal control

In order to command the longitudinal speed of the robot, a Predictive Functional Controller (PFC, [10]) is employed, fed by the previously generated velocity limit profile as reference. The PFC approach thus respects the longitudinal dynamics of the vehicle and calculates the optimum correcting variable to attain the desired speed profile. The internal model of the longitudinal dynamics has been obtained via identification because the actual behavior is rather complex (closed loop control on the vehicle low level + vehicle dynamics). For reasons of simplicity a representation with m equal time constants T has been chosen: $G_{lon}(s) = \frac{K}{(1+T\,s)^m}$. Gain K and an inflection time t_i have been determined from a corresponding step of desired velocity response. For $m = 3$, $t_i = (m-1)\,T$ yields:

$$G_{lon}(s) = \frac{1}{(1 + 0.8\,s)^3} \tag{13}$$

PFC is a receding horizon approach, taking into account h future points in time (coincidence points in sampled time, interval T_s). At instance n the controller will use the sequence $v_d(n+i)$, $0 \le i \le h$ of the desired speed profile as reference. It calculates an optimal sequence $v_s(n+i)$ for the control variable, the speed set point sent to the robot's low level control. The optimization is based on a set of n_B base functions, each of them defined for the h coincidence points:

$$u_B = \begin{pmatrix} u_{B1}(0) & u_{B1}(1) & \dots & u_{B1}(h-1) \\ u_{B2}(0) & u_{B2}(2) & \dots & u_{B2}(h-1) \\ \dots & \dots & \dots & \dots \\ u_{Bn_B}(0) & u_{Bn_B}(2) & \dots & u_{Bn_B}(h-1) \end{pmatrix}$$

The control sequence is determined via the n_B-dimensional weighting vector μ, that is subject of the optimization:

$$v_s(n+i) = \sum_{k=1}^{n_B} \mu_k(n) u_{Bk}(i)$$

This optimal weighting vector needs to be computed at each controller cycle n by minimizing the criterion:

$$D(n) = \sum_{i=1}^{h} \left[\hat{v}(n+i) - v_d(n+i)\right]^2 ,$$

where $\hat{v}$ is the predicted linear velocity of the robot, i.e. the output of the process model (13) to the control sequence v_s. At each cycle only the first element:

$$v_s(n) = \sum_{k=1}^{n_B} \mu_k(n) u_{Bk}(0)$$

is applied to the robot. The strategy is illustrated in Fig. 4

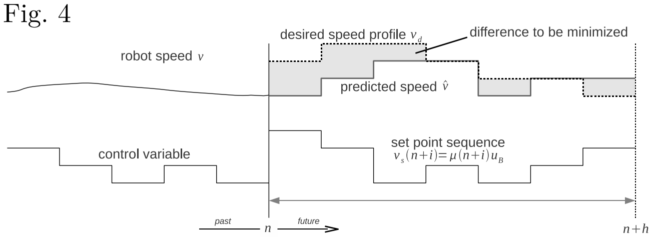

Fig. 4. Illustration of PFC for longitudinal speed control

At every controller step n a new coincidence point $v_d(n+h)$ is determined employing the current friction conditions $C_{F,R}(n)$ and the future curvature $c\big(a(n+h)\big)$, where $a(n+h)$ is calculated by integration of the desired speed $v_d(n+i), 0 \leq i \leq h$. Since $v_d(n+h)$ depends on $a(n+h)$ in turn, the tuple is approximated iteratively. It is not necessary to determine an exact value for $a(n)$, since $c(a)$ develops smoothly (guaranteed by a polynomial approximation of the path). At the same time, values of v_d that exceed the default velocity v_t are omitted.

IV. Experimental results

A. Steering angle limitation

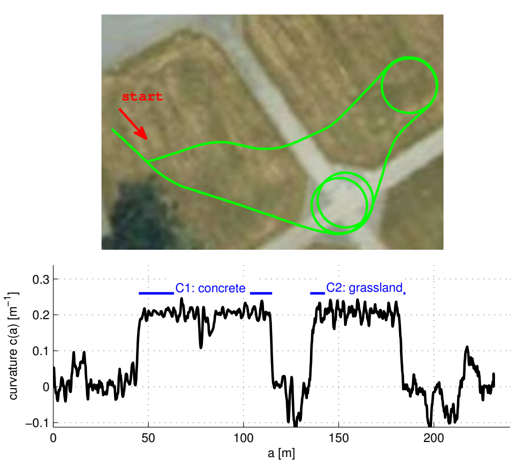

Fig. 5. Reference trajectory and corresponding curvature

The algorithm has been tested in combination with the kinematic path tracking control law and the mixed-mode observation scheme described in section II. A reference path has been chosen so that A) it contains high curvature segments, B) these segments are positioned on two different types of ground (grassland and concrete). Fig. 5 illustrates the shape of the path and the different ground types by an overlay of an aerial view and the corresponding curvature along this path. It indicates the two curved segments C1 and C2 on concrete and on grassland, respectively. The reference path was generated via a learning procedure at low robot speed, thus ensuring its kinematic feasibility.

In order to verify the velocity limitation algorithm, the robot was tracking the reference path at different speeds ($4\,\mathrm{m\,s^{-1}}$ and $5\,\mathrm{m\,s^{-1}}$), with a steering angle limit of $17°$) and with different prediction horizons h (where only the most favorable results of $h = 3\,\mathrm{s}$ are shown here) in the longitudinal speed control. As a reference, the robot was also tracking the path at constant speed.

TABLE II

Value reached by δ for speeds $v_t = 4\,\mathrm{m\,s^{-1}}$ and $v_t = 5\,\mathrm{m\,s^{-1}}$

		reference		**limit 17°**	
		$4\,\mathrm{m\,s^{-1}}$	$5\,\mathrm{m\,s^{-1}}$	$4\,\mathrm{m\,s^{-1}}$	$5\,\mathrm{m\,s^{-1}}$
C1	max(δ)	18.9	19.6	16.9	17.0
	mean(δ)	14.9	15.3	14.9	14.7
C2	max(δ)	20.0	20.3	17.6	17.7
	mean(δ)	15.2	16.9	14.9	14.7

Figs. 6 and 8 show the resulting steering angle for $v_t = 4\,\mathrm{m\,s^{-1}}$ and $v_t = 5\,\mathrm{m\,s^{-1}}$) with limitation enabled and disabled. It can be observed, that the steering angle reaches the physical limit of $20°$ during the reference runs (although it was taught with a maximum steering angle of $15°$). If the speed limitation is enabled, the steering angle stays clearly below this bound. The steering action is lower because of the limitation of the vehicle longitudinal speed (Figs. 7 and 9) by the PFC algorithm, the limitation algorithm works efficiently. The resulting maximum and mean steering angles during the curves C1 ($50 < a < 110$) and C2 ($140 < a < 175$) are summarized in table II.

It is interesting to note the differences between curves C1 and C2: from different tire-ground friction conditions (Fig. 10) different speed limits are arising. For instance

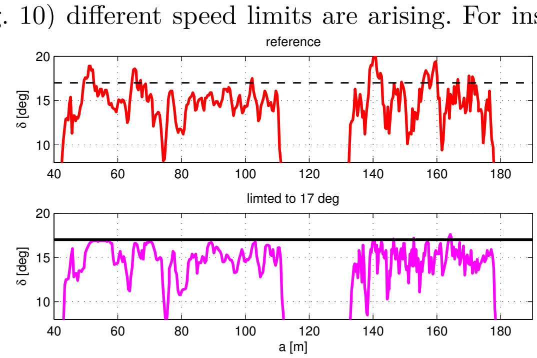

Fig. 6. Measured steering angle in experiment at $4\,\mathrm{m\,s^{-1}}$

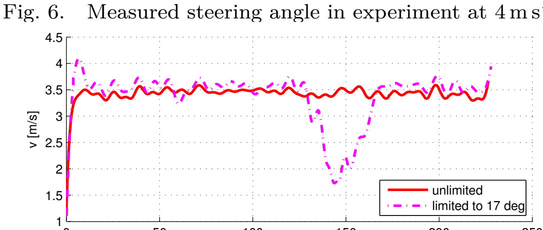

Fig. 7. Measured linear speed in experiment at $4\,\mathrm{m\,s^{-1}}$

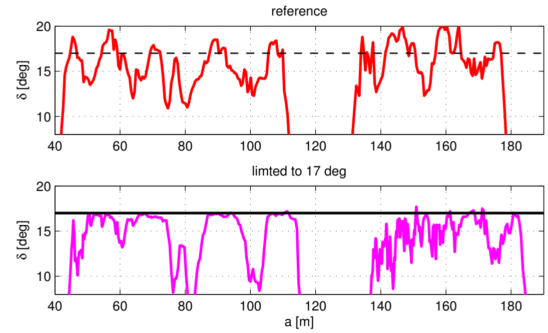

Fig. 8. Measured steering angle in experiment at $5\,\mathrm{m\,s^{-1}}$

for $v_t = 4\,\mathrm{m\,s^{-1}}$ the speed is not limited during C1 but during C2. As shown in Fig. 9, the speed is limited in both curves at $5\,\mathrm{m\,s^{-1}}$. The adaptation of cornering stiffnesses, as described in section II is reported in Fig. 10.

B. Tracking accuracy

The mean tracking error stays quasi constant under limited velocity. Indeed, one would expect a decreasing error when the robot is decelerated, but the speed dependency of the dynamic observers associated with the tracking control causes significant deviations during the transitions between straight and curved path segments. In Fig. 11 the tracking error for $4\,\mathrm{m\,s^{-1}}$ is shown. The re-acceleration of the robot after $a = 170\,\mathrm{m}$ causes oscillations around the path, but they do not exceed the typical error range.

V. Conclusions and future work

The presented algorithm extends the existing off-road mobile robot path tracking strategy to account for steering angle saturation. To this end, the vehicle's longitudinal speed is linked to the turning radius via a steady state equation of the vehicle dynamic behavior. The grip conditions are estimated by an on-line adaptation of the cornering stiffnesses. In this manner, the path tracking control law is preserved, while the constraintness of the primary control variable is respected. The generated velocity target profile is used as reference for a PFC, that

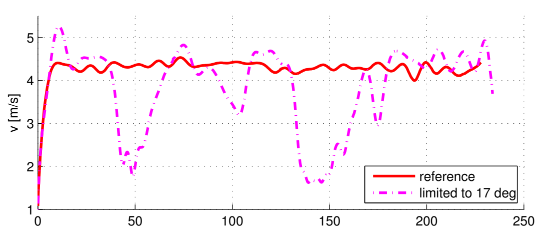

Fig. 9. Measured linear speed in experiment at $5\,\mathrm{m\,s^{-1}}$

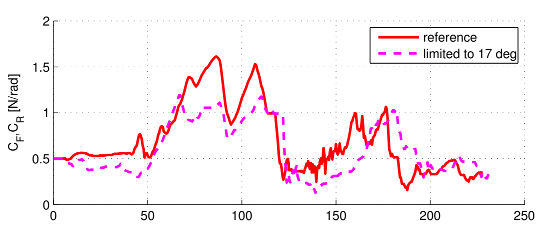

Fig. 10. Cornering stiffnesses for $v_t = 5\,\mathrm{m\,s^{-1}}$ (front wheel)

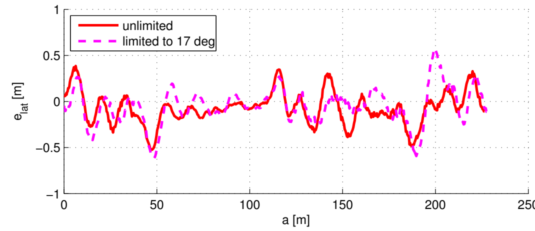

Fig. 11. Tracking error at $4\,\mathrm{m\,s^{-1}}$

takes into account the longitudinal dynamic behavior of the robot.

The effectiveness of the approach was shown via experiments, where the steering properties were compared for different speeds. However, the approach currently suffers from the speed dependency of the present control architecture: predictive steering control and dynamic observers are correlated with the vehicle longitudinal velocity. Since this work is part of a bigger aggregation of stability and safety related algorithms, this problem will be subject of future work. Additionally, the steering actuator is not only constrained in its maximum angle. The steering speed is limited as well, influencing the maneuverability in transient sections when the curvature of the path is changing. To this end, the presented predictive algorithm will be extended to cover these additional constraints in the vehicle dynamics.

This work is related to the project FAST, funded by the French National Research Agency (grant number ANR-07-ROBO-0008, https://projetfast.cemagref.fr).

References

[1] C. Samson, "Control of chained systems: Application to path following and time varying point stabilization of mobile robots," *IEEE Trans. Automat. Contr.*, vol. 40, pp. 64–77, 1995.

[2] M. Ellouze and B. d. Andréa-Novel, "Control of unicycle-type robots in the presence of sliding effects with only absolute longitudinal and yaw velocities measurement." *European Journal of Control*, vol. 6, pp. 567–584, 2000.

[3] R. Lenain, B. Thuilot, C. Cariou, and P. Martinet, "Mixed kinematic and dynamic sideslip angle observer for accurate control of fast off-road mobile robots," *Journal of Field Robotics*, vol. 27, pp. 181–196, 2010.

[4] R. Lenain, B. Thuilot, O. Hach, and P. Martinet, "High-speed mobile robot control in off-road conditions: A multi-model based adaptive approach," accepted for publication at ICRA2011.

[5] C. Connette, A. Pott, M. Hägele, and A. Verl, "Addressing input saturation and kinematic constraints of overactuated undercarriages by predictive potential fields," in *Proc. IROS*, 2010, pp. 4775–4781.

[6] V. Munoz, A. Ollero, M. Prado, and A. Simon, "Mobile robot trajectory planning with dynamic and kinematic constraints," in *Proc. ICRA*, 1994, pp. 2802–2807.

[7] W. Ren, J.-S. Sun, R. Beard, and T. McLain, "Nonlinear tracking control for nonholonomic mobile robots with input constraints: An experimental study," in *Proc. ACC*, 2005, pp. 4923–4928.

[8] C. Wang, "Semiglobal practical stabilization of nonholonomic wheeled mobile robots with saturated inputs," *Automatica*, vol. 44, pp. 816–822, 2008.

[9] R. Lenain, B. Thuilot, C. Cariou, and P. Martinet, "Adaptive and predictive path tracking control for off-road mobile robots," *European Journal of Control*, vol. 13, pp. 419–439, 2007.

[10] J. Richalet, "Industrial applications of model based predictive control," *Automatica*, vol. 29, pp. 1251–1274, 1993.